VERT-X Design of Vertical X-Ray Test Facility for ATHENA

CONCEPT OF OPERATION

Doc: VTX-OAB-IOP-TEC-001

Date: 17 / 04 / 2020

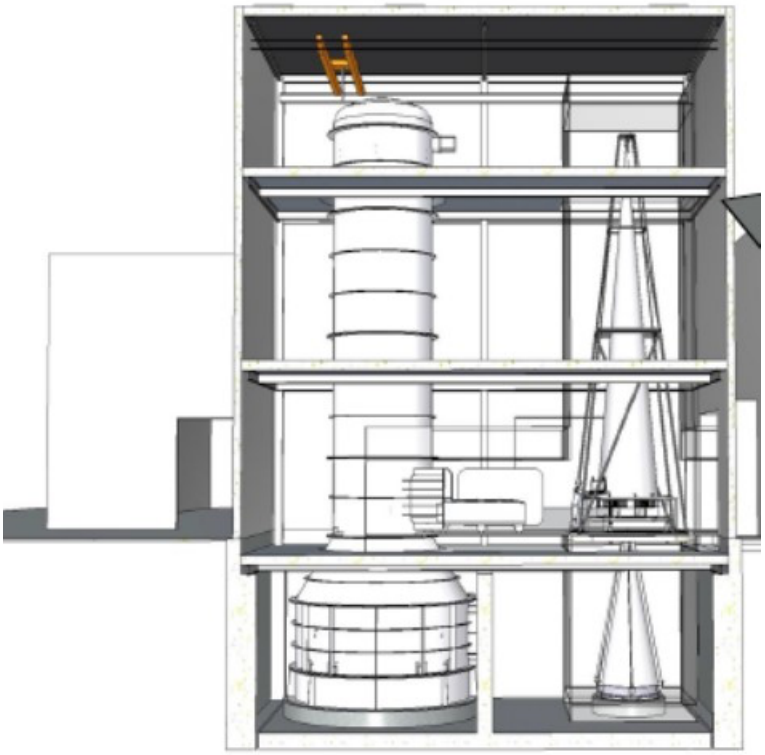

VERT-X Design of Vertical X-Ray Test Facility for ATHENA

CHANGE RECORDS						
ISSUE	**DATE**	**AUTHOR**	**APPROVED**	**QA/QC**	**SECTION / PARAGRAPH AFFECTED**	**REASON/INITIATION Documents/Remarks**
I01p00	23/10/2019				All	First Issue
I01p01	20/12/2019				All	Error budgets moved to TN12
I01p02	17/04/2020				Sect 11	Added Sect 11+ minors

AUTHORS AND RESPONSIBLES			
Document:	VTX-OAB-IOP-TEC-001		
Issue:	I01p02		
Date:	17/04/2020		
Prepared by:	A.Moretti (INAF – OAB)	Signed by :	
	G. Sironi (INAF – OAB)		
	D. Spiga (INAF – OAB)		
Checked by:	Alberto Moretti (INAF - OAB)	Signed by:	
Approved by:	Stefano Basso (INAF - OAB)	Signed by:	
Released by:	Alberto Moretti (INAF - OAB)	Signed by:	

CONTRIBUTING ENTITIES	
INAF – OAB	Partner
INAF - IASF	Partner
Media Lario	Partner
EIE	Partner
GP Advanced Projects	Partner
BCV	External Service

TABLE OF CONTENTS

1. INTRODUCTION

1.1. SCOPE

The scope of the present document is to present the preliminary implementation of the ATHENA mirror verification and calibration plan through the VERT-X calibration facility.

1.2. APPLICABILITY

The present document is one of the Preliminary Design Review (PDR) deliverables. It is intended to be an input to VERT-X preliminary design and a driver for the operations concept development in the next phases of the study.

2. APPLICABLE AND REFERENCE DOCUMENTS

2.1. APPLICABLE DOCUMENTS

AD1	AO/1-9549/18/NL/AR - SOW	X-ray Raster Scan Facility for the ATHENA Mirror Assembly SOW
AD2	VERT-INAFOAB-001	VERTICAL X-Ray (VERT-X) Technical Proposal
AD3	ESA-TECMMO-RS-014713	Updated Requirements for the ATHENA VERT-X following the System Requirements Review

2.2. REFERENCE DOCUMENTS

RD1	VTX-OAB-ISE-REP-001 - Conceptual Design Report
RD2	VTX-OAB-ISE-REP-002 - Trade-off Report
RD3	ATHENA - MCF URD, IRD & ICD ISSUE 1.3 [ESA].pdf
RD4	ATHENA - Calibration Requirements Document, ESA-ATH-SP-2016-001, issue 0.5.1.pdf
RD5	ATHENA - Optics Calibration Plan, ESA-ATHENA-ESTEC-SCI-PL-0001, Issue 1.1.pdf
RD6	ATHENA - Acronyms and Definitions ATHENA-ESA-LI-0001
RD7	VTX-EIE-ISE-TEC-002 Raster Scan System
RD8	VTX-MLT-ISE-TEC-001 X-ray Source and Collimator System
RD9	VTX-OAB-ISE-TEC-001 Technical Budgets
RD10	STRAY-LIGHT simulation, rw_stray_xrays_Feb_2019, Willingale R. 2019
RD11	VTX-OAB-ISE-TEC-001 Xray detector and (x,y,z) stage

2.3. GENERAL SPECIFICATIONS AND STANDARD DOCUMENTS

SD1	ECSS-M-40A	Configuration management
SD2	ECSS-M-50A	Information/documentation management

2.4. LIST OF ACRONYMS

AD	Applicable Document
EA	Effective Area
EIE	EIE Space Technologies
ESA	European Space Agency
GPAP	GP Advanced Projects
IASF	Istituto di AstroFisica Spaziale (INAF, Milano)
INAF	Istituto Nazionale di AstroFisica
MA	Mirror Assembly
MLS	Media Lario S.r.l.
OAB	Osservatorio Astronomico di Brera (INAF, Milano)
PDR	Preliminary Design Review
PSF	Point Spread Function
RD	Reference Document
SD	Standard Document
SIM	Science Instrument Module
SOW	Statement of Work
SRR	System Requirements Review
TBA	To Be Assessed
TBC	To Be Controlled
TBD	To Be Defined
TEC	Technical Note
VERT-X	VERTICAL X-Ray
VTX	VERT-X

3. VERIFICATION REQUIREMENTS

As specified in RD3 during the verification phase the following campaigns are planned:

1. Performance verification campaign tests for the MA QM (**3 months, Oct 2024**);
2. Alignment checks during the MA FM integration campaign (**2 years, Jul/2026**);
3. Performance verification campaign tests for the MA FM (**6 months, Mar/2028**);

These will consist in different sequences of four tests, according the scheme defined in the Integration & Verification flows tab of RD3.

These four different tests are:

- Alignment acceptance (**AA**)
- Intermediate alignment acceptance (**IAC**);
- Abbreviated functional test (**AFT**);
- Full functional tests (**FULL**).

AA coincides with IAC, while FULL will perform the same tests of AFT at three energies instead of 1 energy with the MA TCS operating.

Scope and requirements of the four tests are the following.

AA and **IAC** shall determine:

- The MA optical axis; AKE ≤10" with 68% confidence.
- The MA on-axis A_{eff}; AKE ≤10% with 68% confidence.
- The MA focal length; AKE ≤100μm with 99.7% confidence at one energy (e.g. Al-K)
- The MA on-axis PSF HEW; AKE of ≤2% with 68% confidence.

At 3 energies (unless above otherwise specified, e.g.: C-K. Al-K, Ti-K), under a uniform temperature of 20°C ± TBD°C (thermal conditions mimicking the MM-->MA integration, and nominal flight operation), with the MA TCS not operating.

AFT shall determine:

- The MA on-axis A_{eff}; AKE of ≤10% with 68% confidence.
- The MA on-axis PSF HEW; AKE of ≤2% with 68% confidence.

At 1 energy, under a uniform temperature of 20°C ± TBD°C (thermal conditions mimicking the MM-->MA integration, and nominal flight operation), with the MA TCS not operating.

Full shall determine:

- The MA on-axis A_{eff}; AKE of ≤10% with68% confidence.
- The MA on-axis PSF HEW; AKE of ≤2% with 68% confidence.

At 3 energies (e.g.: C-K, Al-K, Ti-K), under TBD temperature conditions, with the MA TCS operating.

As said, the three verification campaigns will consist in several sequences of these 4 tests according the following scheme as defined in the Integration & Verification flows tab of RD3 (this is an initial

specification of the performance verification requirements of the MA, and will be revised by the Primes):

1. Mirror QM performance: AA+FULL+AFT+FULL on the QM (1,8,15 rows, 2 sextans, 46 modules in total)
2. Mirror FM integration: three repetitions of IAC on FM with 1-3, 1-8, 1-12 integrated rows respectively
3. Mirror FM performance: Consists in the sequence: AA+FULL+AFT+FULL on the FM (15 rows, 6 sextans, 678 modules in total).

The list of the required measures during the verification phase are listed in Table 1.

Table 1 Summary of the Verification tests and corresponding required accuracy [RD3].

WHERE	GOAL	ACCURACY	ENERGY	TESTS	REQ	WHEN	WHAT
On Axis	FOCAL LENGTH	1mm (99.7%)	1 (Al-Kα)	10	LB-URD-365	AA, IAC	QM,FM1-3, FM1-8, FM1-12, FM.
On Axis	OPTICAL AXIS	10'' (68%)	3 (C,Al,Ti-Kα)	15	LB-URD-365-366	AA, IAC	QM, FM1-3, FM1-8, FM1-12, FM.
On Axis	HEW	2% (68%)	1 (C,Al,Ti-Kα)	1	LB-URD-368	AFT	QM, FM1-3, FM1-8, FM1-12, FM.
On Axis	A_{eff}	10% (68%)	1 (C,Al,Ti-Kα)	1	LB-URD-368	AFT	QM, FM1-3, FM1-8, FM1-12, FM.
On Axis	HEW	2% (68%)	3 (C,Al,Ti-Kα)	1	LB-URD-365-366-368-369	AA, IAC, FULL	QM, FM1-3, FM1-8, FM1-12, FM.
On Axis	A_{eff}	10% (68%)	3 (C,Al,Ti-Kα)	1	LB-URD-365-366- 368-369	AA, IAC, FULL	QM, FM1-3, FM1-8, FM1-12, FM.

4. CALIBRATION REQUIREMENTS

In Table 2 we report the calibration requirements which are relevant for the present document, i.e. the ones involving MA testing on ground as reported in RD4.

Table 2 Summary of the on-ground calibration requirement which involve the MA

WHERE	GOAL	ACCURACY	ENERGY	TESTS	REQ
ON Axis	Focal length	1mm (99.7%)	3(Al-Kα,Ti-Kα,Cu-Kα)	10	LB-URD-374 CAL-AST-R-002
On Axis	Optical axis	36" (99.7%)		15	LB-URD-373 CAL-AST-R-005
On Axis	HEW	0.1" (68.3%)	7 (C-K / Ge-K)	1	LB-URD-376 CAL-PSF-R-001
On Axis	PSF	5% (68.3%)	7 (C-K / Ge-K)	1	LB-URD-376 CAL-PSF-R-001
Off-Axis	HEW	0.1" (68.3%)	7 (C-K / Ge-K)	1	LB-URD-376 CAL-PSF-R-001
Off-Axis	PSF	15% (68.3%)	7 (C-K / Ge-K)	1	LB-URD-376 CAL-PSF-R-001
On Axis	A_eff (abs)	6% (68.3%)	10 (TBD 0.2-12.0 keV)	-	LB-URD-379 CAL-EEF_R-001
On Axis	A_eff (rel)	2% (68.3%)	0.2-12.0 keV continuum, step 1/3 spectral resolution	-	CAL-EEF_R-003
Off Axis	A_eff (rel)	3%(68.3%)	0.3-7.0 keV continuum, step 1/3 spectral resolution	-	LB-URD-382 CAL-EEF-R-004
OUT Fov	Stray-light	5% (99.7%)	2 (Al-Kα,Fe-Kα)	10	LB-URD-383 CAL-PSF-R-003
Out focus	HEW	0.5" (99.7%)	Not specified	10	LB-URD-377

5. POINT SPREAD FUNCTION STATISTICAL ERROR

Requirements on the PSF are present both in the AD3 and RD4 with some differences. In AD3, the required uncertainty of the HEW both for the verification and calibration for different energies used, both on- and off-axis angles is 1'', with a goal of 0.5'' at 99.73% confidence. Instead, the RD4 requires an error of 0.1" at 68% confidence together with a 5% uncertainty on the EEF of the wings and the halo. The reason for this, is to keep the uncertainty on the flux measure of a point-like celestial source lower than 1%.

The VERT-X HEW measure is the convolution of the intrinsic HEW with some systematic terms, namely the pointing accuracy of the x-ray beam, the source size and the beam divergence due collimator figure error.
Keeping these systematics at a level of few percent of the HEW_{MA} is extremely beneficial.
First, in the error budget, each term is weighted by its ratio with the HEW itself. Then, each term affects the weight of the statistical error.
While the VERT-X total error budget is discussed and estimated in RD9, in this section we estimate the statistical component, which is the strongly linked with the operation concept.
As explained in the RD9, in the present design the statistical error in the HEW measure is the main error source. It follows that its proper assessment is of particular importance.

We started from the ray-tracing output (Willingale 2019v2.4_PSF_Lorentzian_0_arcmin_1_keV.fits) showed in Figure 1: this has been produced with 1,5 10^6 events at 1 keV energy on axis and contains a full treatment of error terms: (i) in-plane and out-of-plane figure errors/response focal length/kink angle errors; (ii) reflection coating and surface roughness/scattering parameters; (iii) translational integration errors; (iv) rotational integration errors.

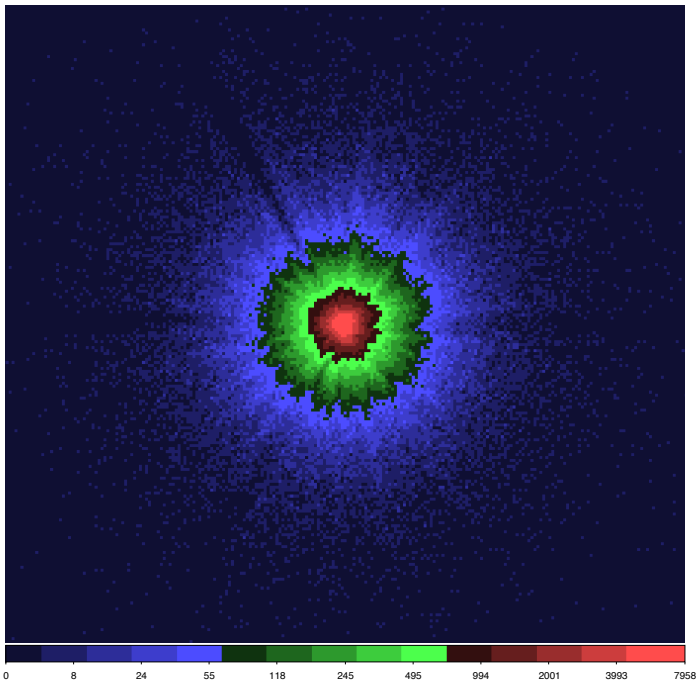

Figure 1 *Output image of a ray-tracing simulation at 1Kev on axis.*

As shown in **Figure 2** we approximate the ray-tracing data with an analytical model which allowed us to extrapolate the PSF up to 10' as required in CAL-PSF-R001. At the moment, for the detector different options with different pixel and sensor sizes are suitable. In the worst case, the detector size (CMOS) will cover 3' at the focal plan (RD1). However, given the very steep slope of the PSF wings we find that the flux fraction beyond 3' is negligible, being < 1%.

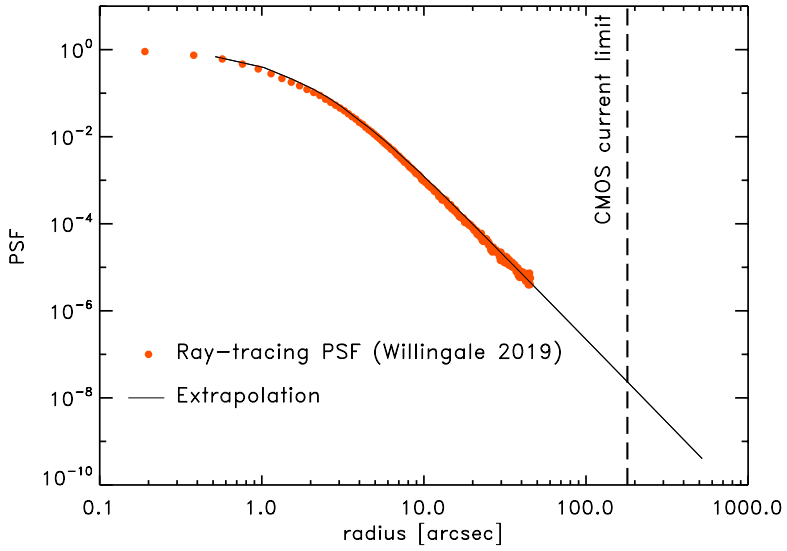

Figure 2 *PSF from ray tracing simulation (red dots) together with analytical model used to extrapolate at larger radii*

PSF model allows us to estimate the expected statistical error in the HEW calibration as function of the number of photons collected during the calibration tests.

To this aim, starting from the analytical model used to fit the ray-racing PSF we simulated PSF with different numbers of photons, ranging from 1000 to 100,000. At a given number of collected events we simulated 100 times PSF and measured the HEW. In **Figure 3**, for each number of photons, we report the standard deviation of the 100 measures. The HEW measure accuracy follows the number of counts with a slope of 0.5: this is expected since the HEW error can be considered as an error on the mean.

In order to keep the statistical uncertainty at the level of 0.1" ~50,000 counts per energy bin are required.

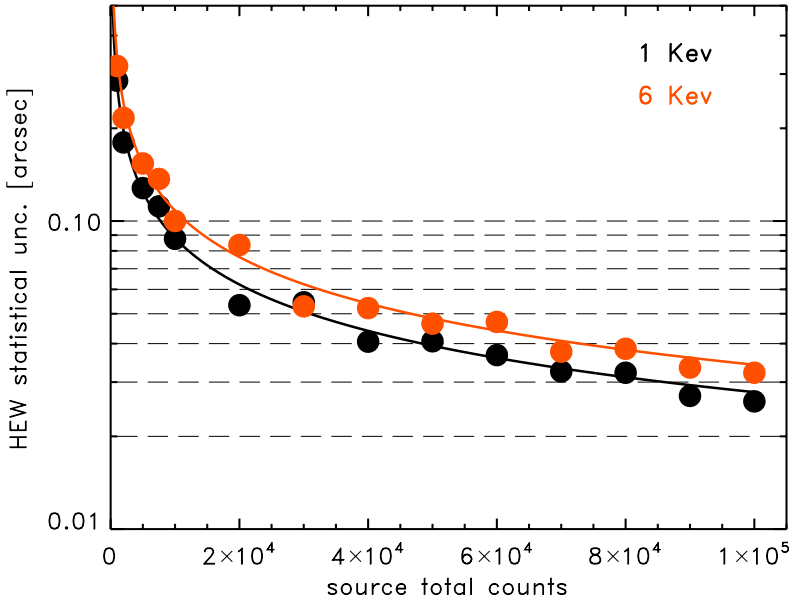

Figure 3 *HEW statistical error as function of collected photons on-axis at two different energies*

Beside the requirement on the HEW, a requirement on the uncertainty of the EEF included in the PSF wings and in the halo is set. The wings and halo are defined as the PSF portion included between 3 and 6 times the HEW and beyond 6 time respectively. The required uncertainties on the corresponding EEF is 5% for both parts. As shown in Figure 4, with the number of photons meeting the HEW requirement (~50,000) we also expect to be compliant with the wing and halo EEF requirements.

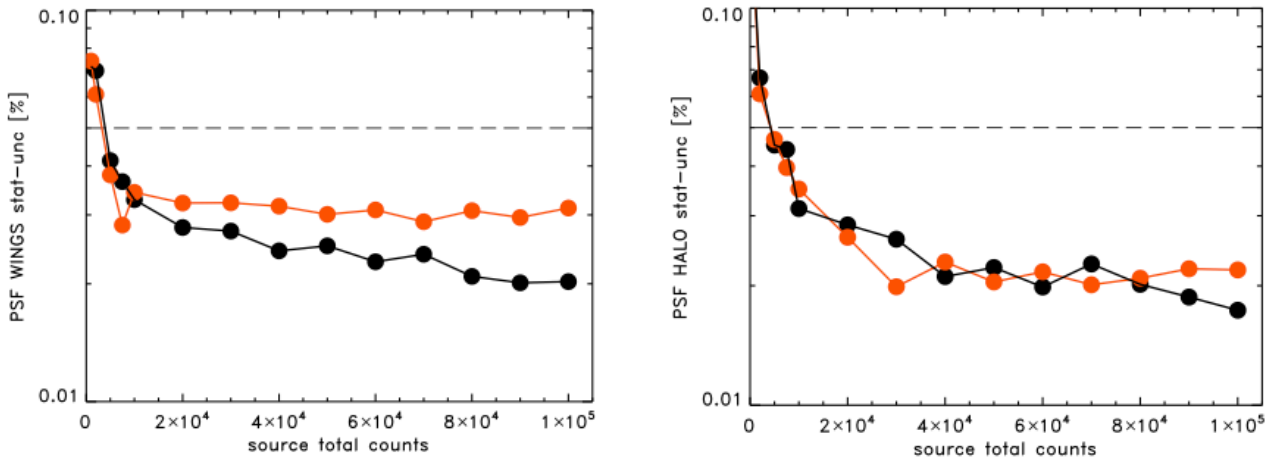

Figure 4 Statistical uncertainty on the EEF included in the wing and in the halo in the left and right panel respectively. Black and red lines and points indicates 1 and 6 keV respectively. Dashed lines show the required accuracy.

6. EFFECTIVE AREA STATISTICAL ERROR

Requirements on EA are given both in terms of absolute and relative calibration.

Absolute calibration of the MA effective area can be achieved by combining measures of the focused beam (R_{foc}), already described in the PSF calibration Section, with measures of the beam directly incident on the detector through the central aperture of the MA (R_{det}) (hereafter flat-field, FF). In this way the EA measure is straightforward. For each energy E, assuming a complete and uniform scan of the area A_{foc} (which includes MA), at uniform velocity, the effective area is given by

$$A_{eff}(E) = A_{foc}\ (C_{foc}(E)/\Delta t_{foc})\ /\ (C_{fla}(E)/\Delta t_{fla})$$

$$A_{eff}(E) = A_{foc}\ R_{foc}(E) / R_{fla}(E)$$

where C_{foc} are the events registered on the detector during Δt_{foc} which is the time spent scanning the area A_{foc} including the MA. C_{fla},Δt_{fla} and R_{fla} are the values relative to the flat-field (FF) measure before, after and during the calibration test.

The required AKE for the absolute measure of the effective area is 6% at 10 monochromatic energies. Systematic error sources are discussed in RD9, while here we discuss the statistical error.

The required AKE for the relative measure of the effective area are 2% and 3% for on- and off-axis measure respectively. Since the relative effective area will be the result of the ratio between focused and direct beams, 5,000 photons for both beams are required. As described in previous Section, for HEW and PSF calibrations a number of 50,000 is required in 1 keV bins. This would mean that the same PSF calibration data-set would provide the needed accuracy for the effective area calibration in bins of 0.1 keV to be compared with the required 0.33 time the WFI spectral resolution.

7. STRAY-LIGHT STATISTICAL ERROR

Required AKE of the stray-light calibration is 5% with a confidence level of at least 99.73%, on scale of 9 arcmin^2 out to an off-axis angle of 20 arcminutes and for energies in the range 0.5–3 keV. Since we expect that stray-light covers 2 quadrants of the FOV, this means that for each out FOV required position, a 20'x10' area should be covered. With the current baseline detector (FOV 8'x8', [RD9]) this means 6-9 different observations with the detector shifted in adjacent positions within the FOV.

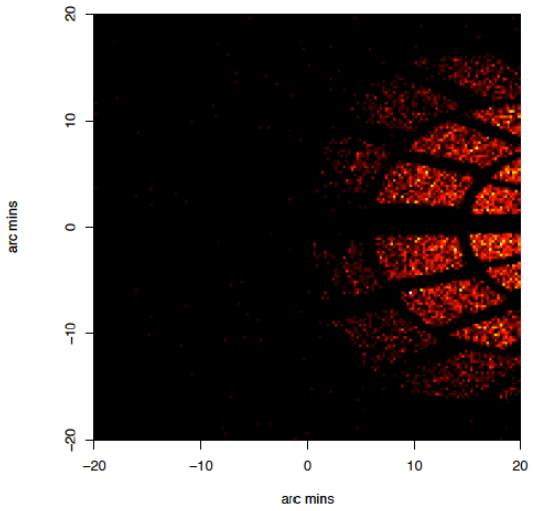

Since the detector area can be covered by 10 9-arcmin^2 circles and that 5% with a confidence level of 99.73%, imposes 1000 counts per circle, a 10x1000 photons should be collected to satisfy the requirement on average for each detector positions.

Since photons are not focused and are spread over the detector area, pile-up is not a limiting factor. The exposure time of these observations is $T_{SCAN.}$ Moreover, since we are not observing a PSF, we can relax the requirement on the pointing accuracy up to 5", we can move the raster scan at maximum velocity of 60 mm/s (RD7).

Total-effective-time-SL = N_{obs} x N_{ene} x T_{SCAN} = 10 x 1 x 9 x T_{SCAN} = 12 days x $(v/20mms^{-1})^{-1}$

8. SYSTEMATIC ERRORS

8.1. EXPOSURE MAP

Ideally, in order to mimic the performance of the optics in astronomical observations, the scan should provide an homogeneous coverage of the whole mirror assembly. Non-homogeneous coverage of the MA would result in a systematic error which could be difficult to evaluate. There are 2 factors acting against homogeneity: geometrical shape of the beam and radial gradient.

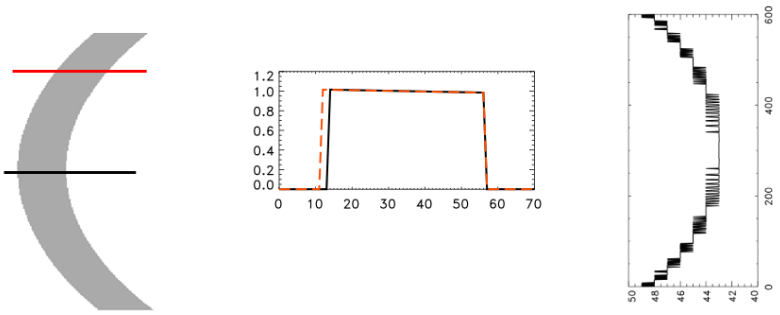

Figure 5 The geometrical shape of the beam.

(i) First, the coverage of the MA is not uniform because the beam size along the scan direction is not uniform, being at maximum at the top and at the bottom of the beam and at minimum in the center, as illustrated in Figure 5. Due to this, those areas of the MA which are scanned by central part of the beam are under-exposed by a factor of 10% with respect to the areas which are scanned by the beam edges, as shown in Figure 6.

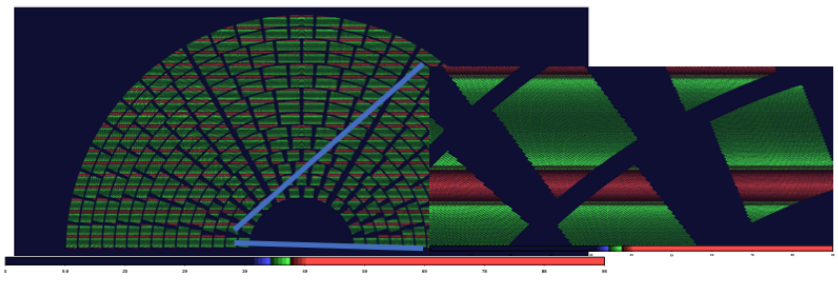

Figure 6 The exposure map of the scan.

(ii) The second factor affecting the coverage homogeneity is the radial gradient which is function of energy. Since the gradient depends on the energy and, as just said, the width of the beam slightly varies along the scan direction this causes a non-uniform coverage of the MA, which has been assessed by means of a ray-tracing simulation. In Figure 7 we plot the footprint of the X-ray beam at four different energies. In the right panel we plot the total intensity of the beam at different

heights. The effect of the gradient on the mean intensity of the beam at different altitudes is negligible everywhere but at the very edges of the beam.

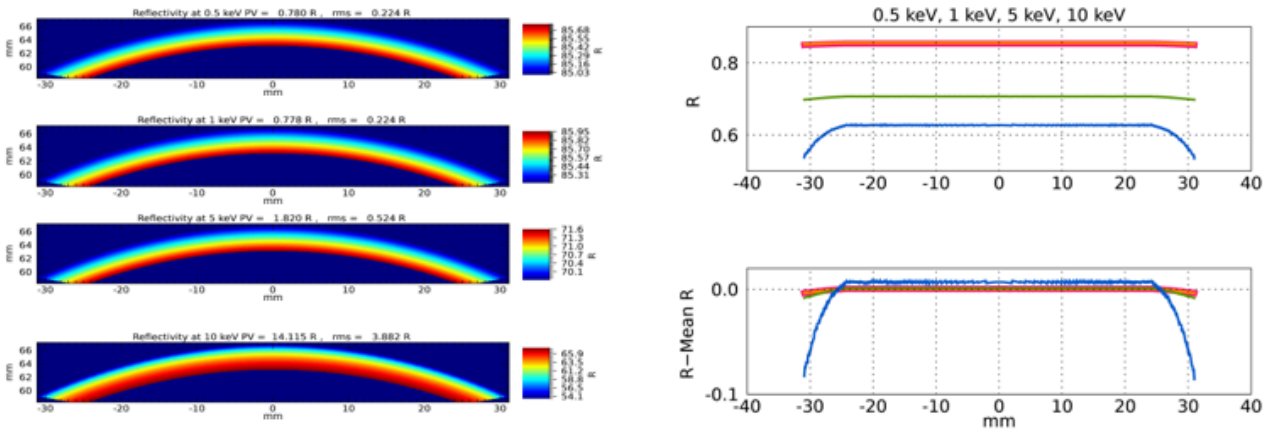

Figure 7 Foorprint at 4 energies.

The edge effect can be removed, shaping the beam in such a way that the two short sides of the corona segments were parallel (Fig. 8). On the other hand, the 10% beam height variation (left panel of Fig. 8) ~10% factor is directly reflected on the homogeneity of the exposure map.

Both these effects can be removed by a mask able to shape the beam in such a way that its width at different heights is constant: this should correct the inhomogeneity of the exposure map, with no side effects.

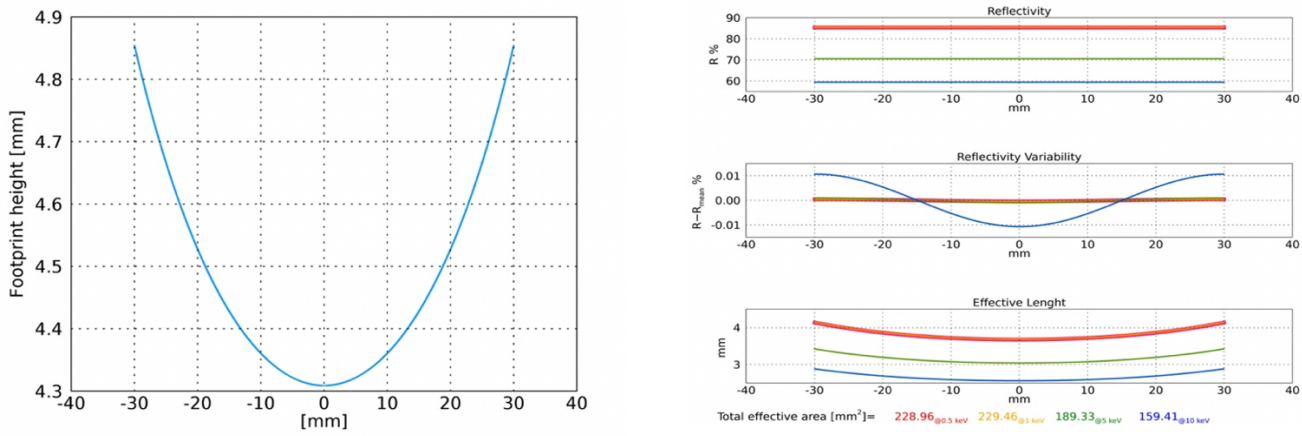

Figura 8 The same of previouse figure in the case of a beam with parallel short sides.

9. PILE-UP

Given that the scan time is of the order of 1.0 hours, the expected limiting factor for the calibration operations is given by the performance of the detector in terms of sustainable flux. Requirements on pile-up fraction is at 1%. Accurate pile-up assessment is therefore mandatory in order to estimate the maximum count-rate suitable in order to meet the requirement. The extreme importance of this estimate is that the calibration duration is linear function of this value.

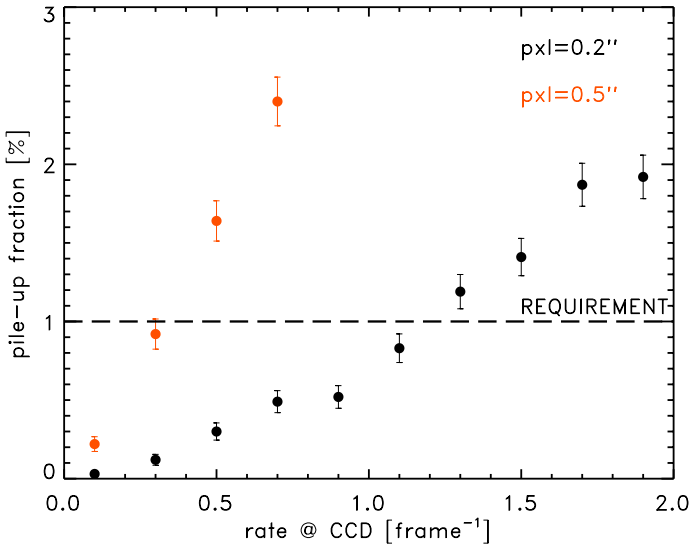

Figure 8 The pile-up fraction two different pixel sizes as function of the count rate per frame of a point-like source (in order to have the count rate of the source this should be multiplied by frame time).

At the moment, for the detector different options with different pixel and sensor sizes are suitable (RD11). In the first option the pixel size is 0.11" with a frame time of 40 s^{-1}. In the second case the pixel size is 0.5" with a frame time of 120 s^{-1}. As it is shown in the plot, in terms of source count rate they yield similar number, which is ~ 40 count s^{-1}. In these simulations we assumed all the events as single pixel events.

10. CALIBRATION OPERATIONS

Given that the necessary amounts of photons are similar, we are planning to use the same data-sets for the aims of both effective area and PSF calibration. Since the required number is much higher than CCD_{RATE} x T_{SCAN}, the limiting factor in this kind of tests is the sustainable count rate.

In the case of Bremsstrahlung continuum, the calculation of necessary exposure time T_{EXP} is not straightforward. This is because photon distribution is not uniform over the required energy band.

In order to calculate T_{EXP} we started from a Bremsstrahlung continuum produced by a target of Ge with KT=40keV and a power of 50W. The spectrum is normalized to match the maximum flux produced by the source (2.6 ph s^{-1} $msterd^{-1}$ mm^{-2} as reported in [RD8]). The spectrum is then multiplied by the effective area of the collimator, which has been calculated as the product of its geometrical area (250 mm^2) with the expected reflectivity, accounting for the double reflections. In order to have the focused photons we multiply by the expected reflectivity of the ATHENA MA and re-normalize the spectrum by a factor of 0.4 to account for geometrical vignetting. Finally, both the simulated focused and direct beams are multiplied by the QE of the detector.

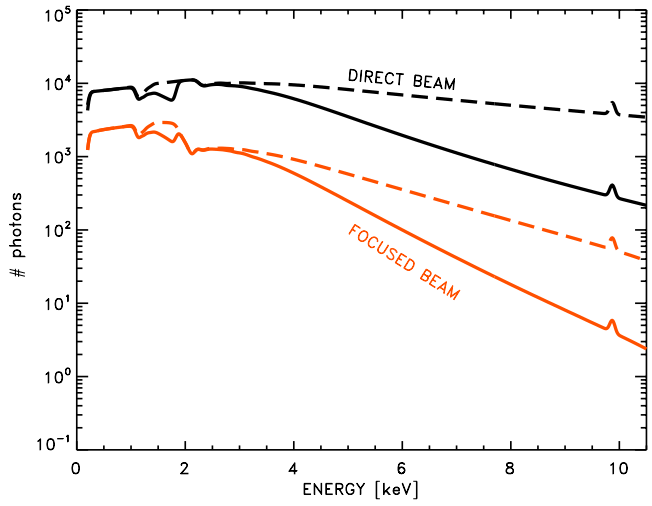

Figure 9. Simulated spectrum of Bremsstrahlung emission including reflectivity and detector QE. Dashed and continuous lines correspond to Sydor and CMOS QE, respectively.

Given the intrinsic spectral shape and the reflections on the collimator and on the MA, for the on-axis observation, where a large coverage is required, it is more convenient splitting the observations in different bands. This can be achieved using high-pass filters like Be window at different thickness levels.

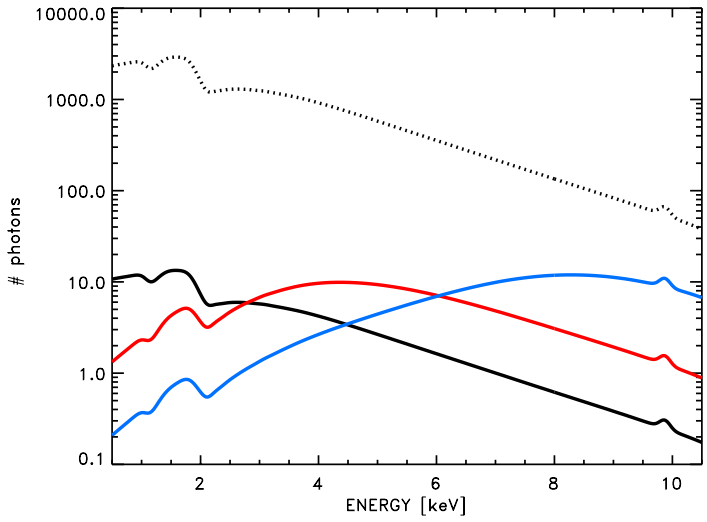

Figure 10. Spectra of direct beam incident on detector with different filters. They are normalized in order to produce the maximum count rate readable by the detector (40 count s^{-1}). While dotted line indicates the spectrum with the source at the maximum intensity level.

The example shown in Figure 10 produces the count distribution shown in Figure 11 in 10 hours with 30% of the time used for the flat field. The core of the calibration campaign will consist in 21 of these observations resulting in a total of 27 days with a day corresponding to 8 hrs.

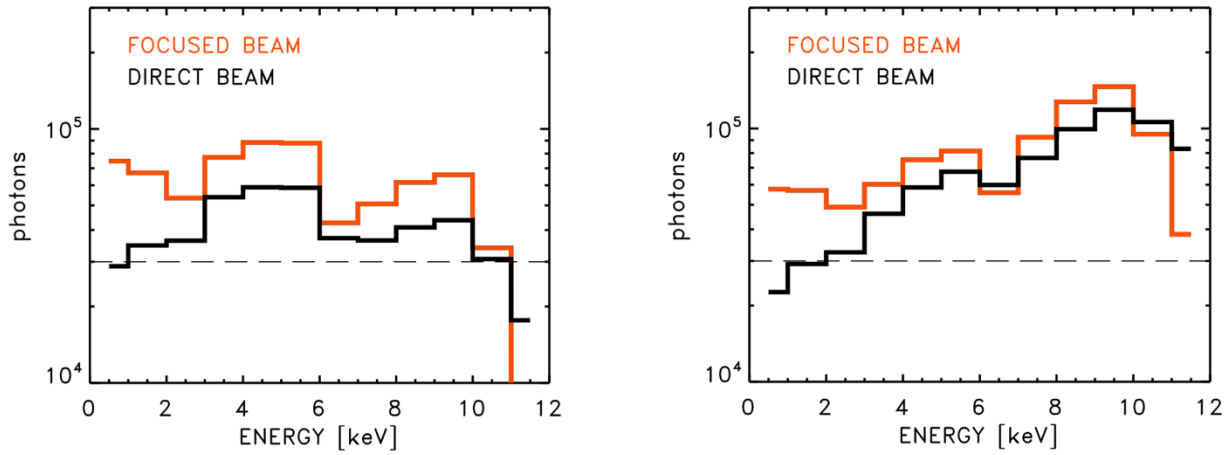

Figure 11Photon distribution registered at the detector in the simulation described in the text and previous figure. Left panel assumes the CMOS QE, while right panel SYDOR QE

These numbers should be considered as preliminary. Improvements in the accuracy of this estimate will come as output of an optimization process which should includes: number of filters, filter energies, exposure time for each filter and flat-field observation.

11. CHARACTERIZATION OF THE SINGLE MODULES

The small size of the VERT-X parallel beam, in principle, allows the characterization of the single modules PSF and effective area. Assuming a scan velocity of 10 mm/s, even the in the worst case, with a detector time frame of 0.025 s we would have a spatial resolution of 250 micron which is largely adequate to map the single modules contribution.

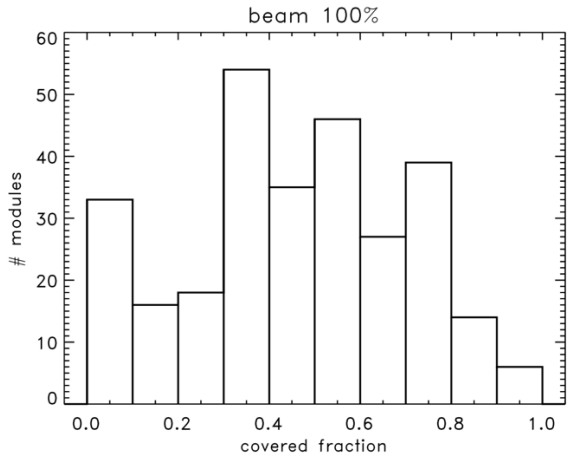

Figura 10 Given a typical path of the raster-scan the histogram of fractions of each module "uniquely" covered.

However, according to the current baseline the beam is of the same size of the single modules and is significantly larger than the ribs. This would prevent this kind of test. We simulated a path for the scan and we registered which fraction of each module uniquely covered, which is the fraction of each module covered by the beam without touching any other adjacent module.

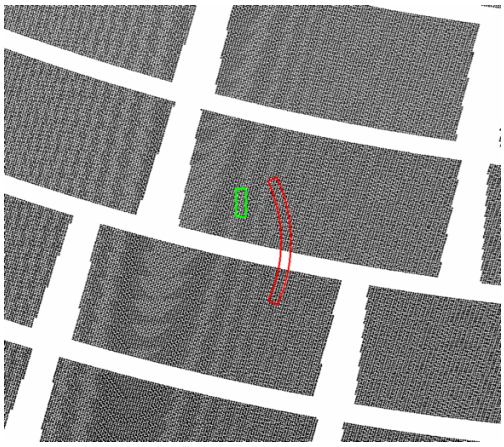

Figura 11 Different sizes of the beam. Red is the baseline (~ 6cm height) ; green is the beam with the reduced size for the purpose of the single module characterization test.

As shown in Fig 10 only a minor fraction of the module is covered by a fraction larger than 90%, resulting in a very poor characterization. On the contrary with, reducing the beam to the 20% of the baseline size (Fig.11) we can obtain an adequate characterization of each single module, as shown

in Fig 12. This shows that with an opportunely reduced beam virtually all the modules can be characterized with 97% of the modules being uniquely covered for fraction higher than 98%.

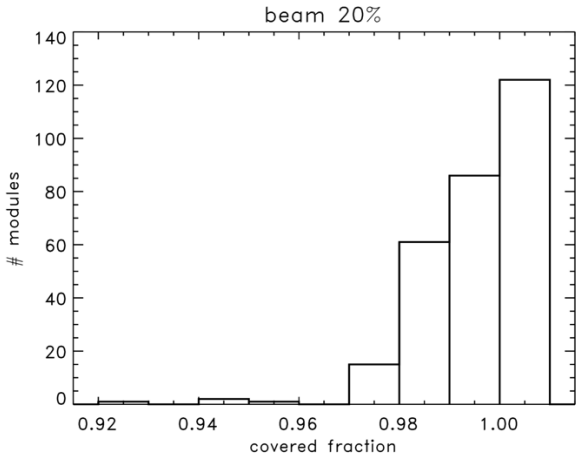

-- END OF DOCUMENT –